A Lithium ion selective membrane synthesized from a double layered Zr-based metal-organic framework (MOF-on-MOF) thin films

(Manuscript No.: DES-D-21-01782)

Huan Xiao[a,1], Milton Chai[b,1], Mojtaba Abdollahzadeh[c], Hadi Ahmadi[c], Vicki Chen[b], Damian B. Gore[a], Mohsen Asadnia[c,*], Amir Razmjou[d,e,f,*]

[a]School of Natural Sciences, Macquarie University, Sydney, New South Wales 2109, Australia
[b]School of Chemical Engineering, University of Queensland, Brisbane, Queensland 4072, Australia
[c]School of Engineering, Macquarie University, Sydney, New South Wales 2109, Australia
[d]School of Engineering, Edith Cowan University, Joondalup, Perth, WA 6027, Australia
[e]Centre for Technology in Water and Wastewater, University of Technology Sydney, New South Wales 2007, Australia
[f]UNESCO Centre for Membrane Science and Technology, School of Chemical Engineering, University of New South Wales, Sydney, NSW 2052, Australia

[1] These authors contributed equally.

Abstract

The ever-growing global demands for lithium (Li^+) require energy-efficient techniques to separate lithium from natural resources and commercial wastewaters. We propose a facile seed-assisted in-situ growth method to prepare double layered UiO-66-based (-$(COOH)_2$ and -NH_2) membranes for Mg^{2+} and Li^+ separation in brine. These membranes, with sub-nanometer-sized windows, nanometer-sized cavities, and functional groups can selectively transport K^+, Na^+, Li^+ over Mg^{2+} and Ca^{2+}. A carboxyl-functionalized UiO-66-based membrane showed higher Li^+ and Mg^{2+} selectivity (up to 90.8) than a UiO-66-NH_2 membrane (65.0) by the current-voltage method using single salt solutions. Carboxylic groups greatly enhance membrane selectivity for Li^+ over Mg^{2+}. The effects and mechanisms of (i) different feed concentrations in a mono-ion system, and (ii) concentration gradients and electrical potential as driving forces for Li^+ extraction in a synthetic multi-ion brine, are discussed. The UiO-66-$(COOH)_2$/UiO-66-NH_2 aluminum oxide membrane exhibited excellent Mg^{2+}/Li^+ separation efficiency in synthetic Qinghai Taijiner Salt Lake brine (abbreviated as Taijiner brine) under concentration gradients. This research will promote metal-organic framework-based membrane designs with tailored pore morphologies and provide an innovative and eco-friendly solution for Li^+ enrichment from salt-lake brines.

Keywords: **UiO-66; Ion selective membrane; Direct lithium extraction; Taijiner brine**

1. Introduction

Global lithium (Li^+) demand has increased 6% per year in recent years and is estimated to reach 95,000 tons per year in 2025 due to fast-growing market demand [1]. Lithium is widely used in rechargeable lithium-ion batteries, nuclear fusion fuels, energy storage materials, aerospace alloys, glass and ceramics, pharmaceuticals and other materials [2, 3]. Aqueous lithium resources comprise about 60% of global reserves, with the remainder in mineral deposits, including brine evaporites and lithium ores. These aqueous lithium resources are concentrated in Bolivia, China, Chile, and the USA in deposits that are more accessible than most mineral ores [4]. Qinghai Lake, the largest alkaline salt lake in China, holds huge lithium reserves that could be exploited [5]. However, lithium extraction from brines is challenging due to their chemically different characteristics, including large concentrations of Mg^{2+} and coexistence with chemically similar ions, particularly K^+ and Na^+. Conventional technologies, including adsorption, precipitation, solvent extraction, ion exchange [6, 7], and electrodialysis to separate lithium from brine, are complex, constrained by complicated processes and pre-treatment requirements. These usually create large amounts of waste and high industrial-scale production costs [8-11]. Thus, developing customized and energy-efficient technologies for lithium recovery from high Mg^{2+}/Li^+ ratio brines is highly attractive.

Membrane technologies have extensive water treatment potential with the easy, environmentally friendly operation and low energy consumption [12-16]. Among membrane processes, nanofiltration can separate Li^+ ions from divalent ions [17-19]. To improve selectivity, scalability and applicability of membranes for Li^+ extraction from various brines, rational design of membranes is critical. Nanostructured membranes can be fine-tuned for selective separation of Li^+ ions from individual brines by adjusting their nanochannel structure and chemistry (e.g. channel morphology, interlayer spacing and inner surface charge) to promote membrane performance [13].

Metal-organic frameworks (MOFs) have high crystallinity, large porosity and tunable functional groups, making them potential materials for customizing membrane pore structures and chemistry and optimizing membrane performance for different environmental applications [20-24]. Recent studies of MOF-based membranes for ion-selective transportation in aqueous solutions mainly discussed design concepts of well-designed pore systems, synthesis routes, filtration performance and the underlying separation mechanisms [25]. A series of MOF-based membranes (e.g. ZIF-8/GO/aluminum oxide, UiO-66s/polyethylene terephthalate and

MOFs/polyvinyl chloride hybrid membranes) were investigated for metal ion selectivity and permeability [26-29]. UiO-66 with high tunability, excellent hydro-stability, simple and commercially viable syntheses are the most representative MOFs that have been developed for fabrication of UiO-66-based membranes (e.g. UiO-66-SO_3H, UiO-66-NH_2 and UiO-66(Zr/Ti)-NH_2 membranes) for efficient ions separation [30-32]. Using guest molecules with an affinity toward specific ions is an effective way to make ion-selective membranes. For example, sulfonate groups of HKUST-1/polystyrene sulfonate/aluminum oxide membranes that exhibit binding affinity to Li^+ over other metal ions have been suggested [33]. Another highly tunable MOF-on-MOF structure strategy has been proposed to create membranes with angstrom-scale asymmetric pores to enhance monovalent ion separation [34]. These findings developed various MOF-based membranes with tailored sub-nanometer pore systems for ion separation applications. Although these hybrid membranes for Li^+ separation are promising, several challenges need to be addressed: (i) poor permeability and selectivity in many polymeric membranes, (ii) polymeric aging, (iii) poor adhesion of MOF-to-substrate and MOF dispersion in MOF-based membranes, and (iv) lack of general and specific understanding of Li^+ transportation behavior in membrane nanochannels from specific brines [35]. Efforts to solve these problems are a significant focus on MOF-on-MOF membrane design with tailored pore morphology and surface charge, in conjunction with improving Li^+ separation performance in brine.

Herein, we report a novel MOF-on-MOF membrane (UiO-66-$(COOH)_2$/UiO-66-NH_2 membrane) constructed by a twin metal ion and different ligands via seeded-assisted in-situ growth. By modifying the media layer of a double layer UiO-66-based membrane with other functional groups (-$(COOH)_2$ and -NH_2), the selectivity for Li^+ will be adjusted. Li^+ transport behavior in membrane nanochannels with different surface charge polarity, feed concentrations and driving forces (e.g. concentration-driven or electrically-driven forces) and underlying mechanisms of Li^+ extraction will also be systematically investigated and elucidated. It is the first study of UiO-66-$(COOH)_2$/UiO-66-NH_2 aluminum oxide (AAO) membranes to extract low concentrations of Li^+ from the representative Taijiner brine (Qinghai Salt Lake, China, [36]), which contains a relatively high Mg^{2+}/Li^+ molar ratio. Our findings will inspire MOF-based membrane designs, optimize ion-selective membrane architecture and functionality, explore universal guidelines for lithium extraction in future industrial production and help boost the circular economy.

2. Experimental

2.1 Materials, chemicals and model brine

Tris(hydroxymethyl)aminomethane (Tris, ≥99.8%), dopamine hydrochloride (PDA, ≥98%), polyethyleneimine (PEI, M_W=800), 2-aminoterephthalic acid (99%), hydrochloric acid (HCl, 37% w/w), pyromellitic acid (95%), *N, N*-dimethylformamide (DMF, 99.8%), ethanol (100%, undenatured), lithium chloride (LiCl, anhydrous, 99.98%), sodium chloride (NaCl, anhydrous, 99.7%), potassium chloride (KCl, 99.0-100.5%), magnesium chloride hexahydrate ($MgCl_2 \cdot 6H_2O$, 98-101%) and calcium chloride ($CaCl_2$, ≥99.9%) were purchased from Sigma Aldrich and zirconium(IV) tetrachloride ($ZrCl_4$, ≥99.5%) was supplied by Alfa Aesar. The flat anodized aluminum oxide membrane (α-Al_2O_3, hydrophilic, pore size: 0.22 μm) was purchased from Whatman. The Poly(dimethylsiloxane) (PDMS) was created by curing Sylgard 184, supplied by Dow Corning Australia. Milli-Q water (Merck Millipore) was used throughout this research. Ion concentrations and Mg^{2+}/Li^+ molar ratios of wide-ranging brines are compared in Table 1 [36-38]. Synthetic Taijiner brine containing a high Mg^{2+}/Li^+ ratio from this typical Chinese salt lake was investigated in this study [5, 22].

Table 1. Ion concentrations of different sources and synthetic Taijiner brine [36-38].

Source	Na^+ mol L^{-1}	K^+ mol L^{-1}	Ca^{2+} mol L^{-1}	Mg^{2+} mol L^{-1}	Li^+ mol L^{-1}	Mg^{2+}/Li^+ molar ratio	Reference
East Taijiner brine	5.094	0.09701	0.01083	0.2321	0.02031	11.42	Sun et al. 2015 [36]
West Taijiner brine	4.454	0.2161	0.004915	0.632	0.03689	17.13	Sun et al. 2015 [36]
Synthetic East Taijiner brine	5.066	0.09949	0.009631	0.238	0.01902	12.51	Sun et al. 2015 [36]
Synthetic West Taijiner brine	4.376	0.2328	0.004267	0.633	0.03487	18.15	Sun et al. 2015 [36]
Raw brine 1	4.585	0.2498	0.08605	0.6871	0.121	5.677	Cha-umpong et al. 2021 [38]
Raw brine 2	4.133	0.2498	0.08605	0.7159	0.1095	6.537	Cha-umpong et al. 2021 [38]

Taijiner, China	2.449	0.1125	0.0049902	0.8311	0.04467	18.606	An et al. 2012 [37]
Salar de Atacama, Chile	3.958	0.6036	0.01123	0.39703	0.2262	1.76	An et al. 2012 [37]
Salar de Uyuni, Bolivia	3.071	0.2992	0.0076351	0.2674	0.04625	5.782	An et al. 2012 [37]
Bonneville, USA	3.61	0.1279	0.001422	0.1646	0.0008213	200.38	An et al. 2012 [37]
Synthetic Taijiner brine	2.74	0.233	0.0107	0.579	0.0279	20.75	**This work**

2.2 Preparation of membranes

2.2.1 Mussel-inspired PDA/PEI modification of AAO membrane

The PDA/PEI coating method has been described previously as a pathway to nucleate formation of MOF coatings [39, 40]. The AAO membrane was immersed in a 50 mM Tris-HCl buffer (pH 8.5) mixing 2 mg mL^{-1} of PDA and 2 mg mL^{-1} of PEI for 4 hours. The modified membrane was immersed in Milli-Q water overnight to eliminate chemical residues and then dried at room temperature.

2.2.2 UiO-66-$(COOH)_2$/UiO-66-NH_2 membrane synthesis

0.131 g of $ZrCl_4$ (0.56 mmol) and 0.2 g of pyromellitic acid (0.79 mmol) were mixed in two separate 20 mL aqueous solutions as metal and ligand precursor solutions of UiO-66-$(COOH)_2$. The precursor solutions were stirred and then poured into a Teflon-lined hydrothermal autoclave vessel along with a PDA/PEI modified AAO membrane, and the reagents were heated at 80 ºC for 3 h. This synthesis step was repeated for another cycle.

The UiO-66-NH_2 layer was created on the UiO-66-$(COOH)_2$ seed layer, which shares the same zirconium node. The metal precursor solution for UiO-66-NH_2 was prepared by mixing 0.2067 g of $ZrCl_4$ (0.89 mmol) in the solvent mixture of DMF (16.7 mL) and HCl (3.3 mL). 0.2267 g of 2-aminoterepthalic acid (1.25 mmol) was blended in 20 mL of DMF to prepare the linker solution. The precursor solutions were homogenously mixed and transferred into a Teflon-lined hydrothermal autoclave vessel along with the UiO-66-$(COOH)_2$ membrane and then heated at 80 °C for 2 h. The UiO-66-NH_2 coating was repeated for another cycle. Steps taken to synthesis the UiO-66-$(COOH)_2$/UiO-66-NH_2 membranes are in Fig. 1.

2.2.3 UiO-66-NH_2 membrane synthesis

The metal precursor solution for UiO-66-NH_2 was obtained by mixing 0.2067 g of $ZrCl_4$ (0.89 mmol) in the solvent mixture of DMF (16.7 mL) and HCl (3.3 mL) as a coordination modulator and the linker solution was synthesized by dissolving 0.2267 g of 2-aminoterepthalic acid (1.25 mmol) in DMF (20 mL). The mixture of precursor solutions was also stirred and poured into a Teflon-lined hydrothermal autoclave vessel with a PDA/PEI modified AAO membrane at 80 °C for 2 h. The UiO-66-NH_2 coating was repeated for another three cycles.

2.3 Fabrication of measuring device

The UiO-66-$(COOH)_2$/UiO-66-NH_2 and UiO-66-NH_2 membranes were cut into 5×10 mm rectangles, then the edges of the membrane were immersed in a 10:1 ratio of PDMS/curing agent and oven-dried for 2 h at 60 ℃. UiO-66-$(COOH)_2$/UiO-66-NH_2 and UiO-66-NH_2 membranes with a size of 1 mm^2 were prepared for testing.

2.4 Characterization

Morphologies of the membrane were characterized by field emission scanning electron microscopy (FEI NanoSEM 230/450). The elemental distribution of the membrane samples was determined through energy-dispersive X-ray spectrometry (EDS) coupled with NanoSEM fitted with a Bruker SDD-EDS detector at 15 kV. Before SEM and EDS analysis, the membrane samples were covered with 20 nm carbon coating. Crystallographic data of the UiO-66 membranes were obtained using a Malvern Panalytical Empyrean I Thin-Film X-ray diffractometer (XRD) through an angle of 5 to 50º2θ with a step size of 0.06º and 300 s per step. Diffractograms were analyzed using Panalytical's High Score Plus software with ICDD PDF-4 database. Analyses of surface chemistry of the membranes were carried out via Fourier transform infrared spectroscopy (FTIR, Bruker Alpha II) in attenuated total reflectance (ATR) mode. Thermogravimetric analyses (TGA) were operated using a TGA Q5000 in an N_2/air environment at temperatures ranging from 25 to 600 °C at 10 °C min^{-1}.

2.5 Selective ion transport properties

The electric-field-driven ion transport in UiO-66-$(COOH)_2$/UiO-66-NH_2 and UiO-66-NH_2 membranes was analyzed by linear sweep voltammetry (LSV) using the ionic strength of 0.01 M chloride salt solutions (e.g., LiCl, NaCl, KCl, $CaCl_2$ and $MgCl_2$) and an H-cell (Fig. 1). The potential was changed from -1 to +1 volt at 100 mV sec^{-1} and the response was recorded. The slope of the current-voltage curve is the conductance of the membrane, divided by the membrane's dimensions, giving the membrane conductivity. Silver/silver chloride electrodes were used for all experiments.

The ion selectivity ratio of Li^+ over other metal ions were calculated as the ratio of measured conductance of the membrane for various cations at the same ionic strength of 0.01 M according to equation 1 [13, 17]:

$$Ion\ selectivity\ ratio = \frac{G_{LiCl}}{G_{other\ ions}} \quad (1)$$

where G_{LiCl} and $G_{other\ ions}$ are the conductance for Li^+ and other ions including K^+, Na^+, Ca^{2+} and Mg^{2+}.

2.6 Ion diffusion

Experiments were performed using an H-cell at room temperature. UiO-66-$(COOH)_2$/UiO-66-NH_2 membranes were embedded between two reservoirs filled with an aqueous salt solution (LiCl or $MgCl_2$ separately, at concentrations of 0.0001, 0.01, 0.1 mol L^{-1}) and Milli-Q water, respectively. The Mg^{2+}/Li^+ selectivity was calculated by the following equation [33]:

$$Selectivity = \frac{C_{Mg2+}}{C_{Li}}$$

where C_{Mg2+} and C_{Li+} are the concentration of Mg^{2+} and Li^+ in permeates at different intervals (0.5, 1, 2, 3, 4, 5 h) and measured by A Mettler Toledo electrical conductivity analyzer.

2.7 Lithium recovery from brine

The composition of synthetic Taijiner brine, in which the solutions were modeled after comparing different sources, is in Table 1. The molar ratio of Mg^{2+}/Li^+ in the synthetic Taijiner brine was 20.75, and other compositions of real brines had ratios ranging from 1.8 to 200.

Concentrations of Na^+, K^+, Li^+, Ca^{2+} and Mg^{2+} in the permeate at different intervals were analyzed using an Agilent 4100 microwave plasma atomic emission spectrometer (MP-AES). The diffusion coefficient (D, $cm^2\ s^{-1}$) was estimated using Fick's law [29];

$$\ln\left(\frac{C_0-2C_t}{C_0}\right) = -\frac{2SD}{VL}t \qquad (2)$$

where C_0 (mol L^{-1}) and C_t (mol L^{-1}) are the concentrations of metal ions in the feed side at the initial time and receiving side at a test time, respectively, S is the effective membrane area (0.01 cm^2), L (50.25 µm) is the membrane thickness, V (50 mL) is the solution volume and t (h) is the test time.

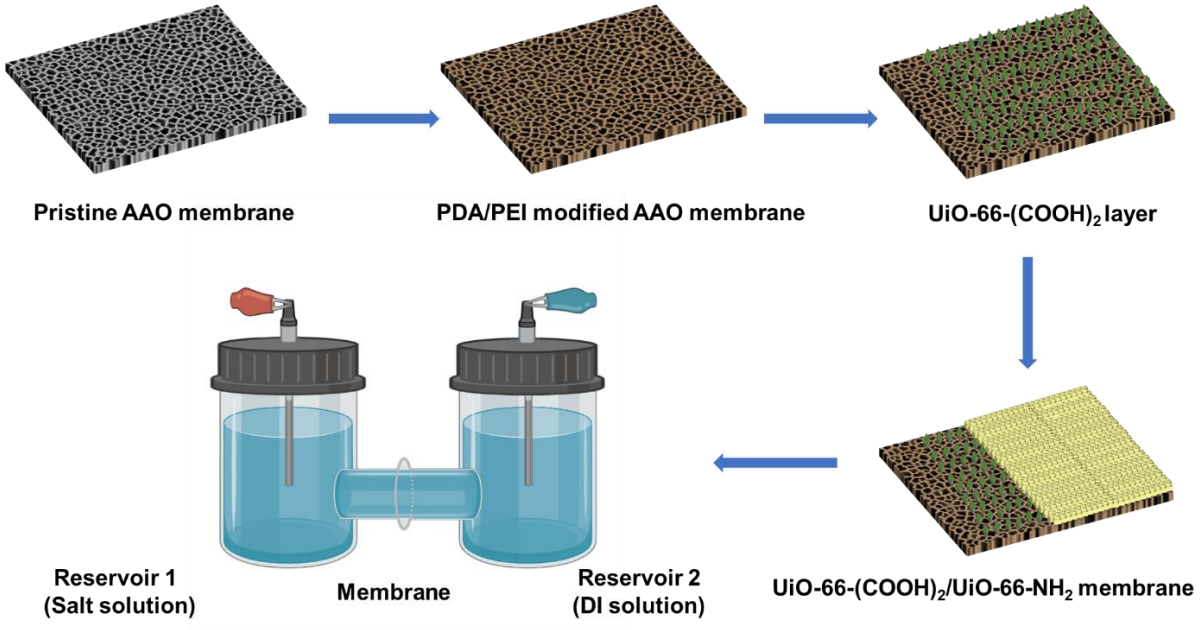

Fig. 1. Schematic of membrane preparation and ion transfer test in an H-cell.

3. Results and discussion

3.1 Characterization of UiO-66-$(COOH)_2$/UiO-66-NH_2 AAO membrane

Surface morphologies of the pristine and modified AAO membranes and cross-sectional morphologies of Zr-based membranes at the different stages are in Fig. 2 and Fig. 3. Modification of the AAO membrane with PDA/PEI can provide an abundance of catechol and amino groups for the nucleation and growth of the MOF film [39-41]. However, it is unlikely that this modification alone can affect ionic separation due to the large membrane pore size of 0.2 µm, as evidenced by the ack of ion selectivity (Li^+/Mg^{2+}) for this membrane in a previous

212 study [34]. The formation of UiO-66-$(COOH)_2$ on the PDA/PEI modified membrane resulted
213 in small seed-like particles on the substrate (Fig. 2. and Fig. 3e). Subsequent growth of UiO-
214 66-NH_2, which had the same Zr metal node as the UiO-66-$(COOH)_2$ seed layer, formed a
215 continuous film on the membrane.

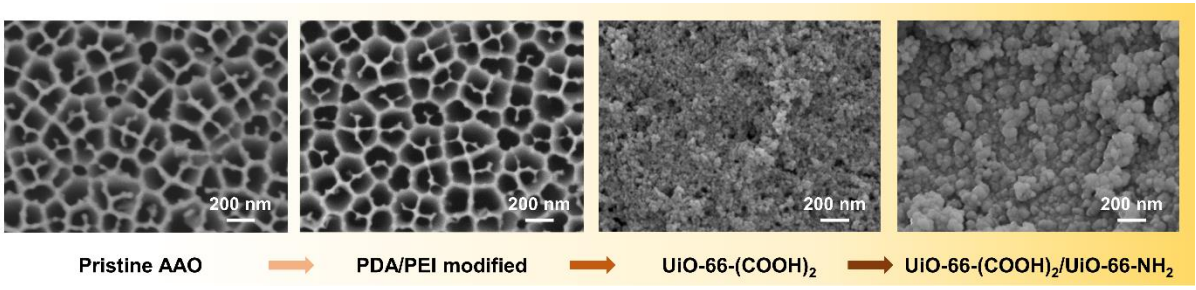

216

217 **Fig. 2.** SEM images of pristine AAO, PDA-PEI modified AAO, UiO-66-$(COOH)_2$ seed layer
218 and UiO-66-$(COOH)_2$/UiO-66-NH_2 membranes.

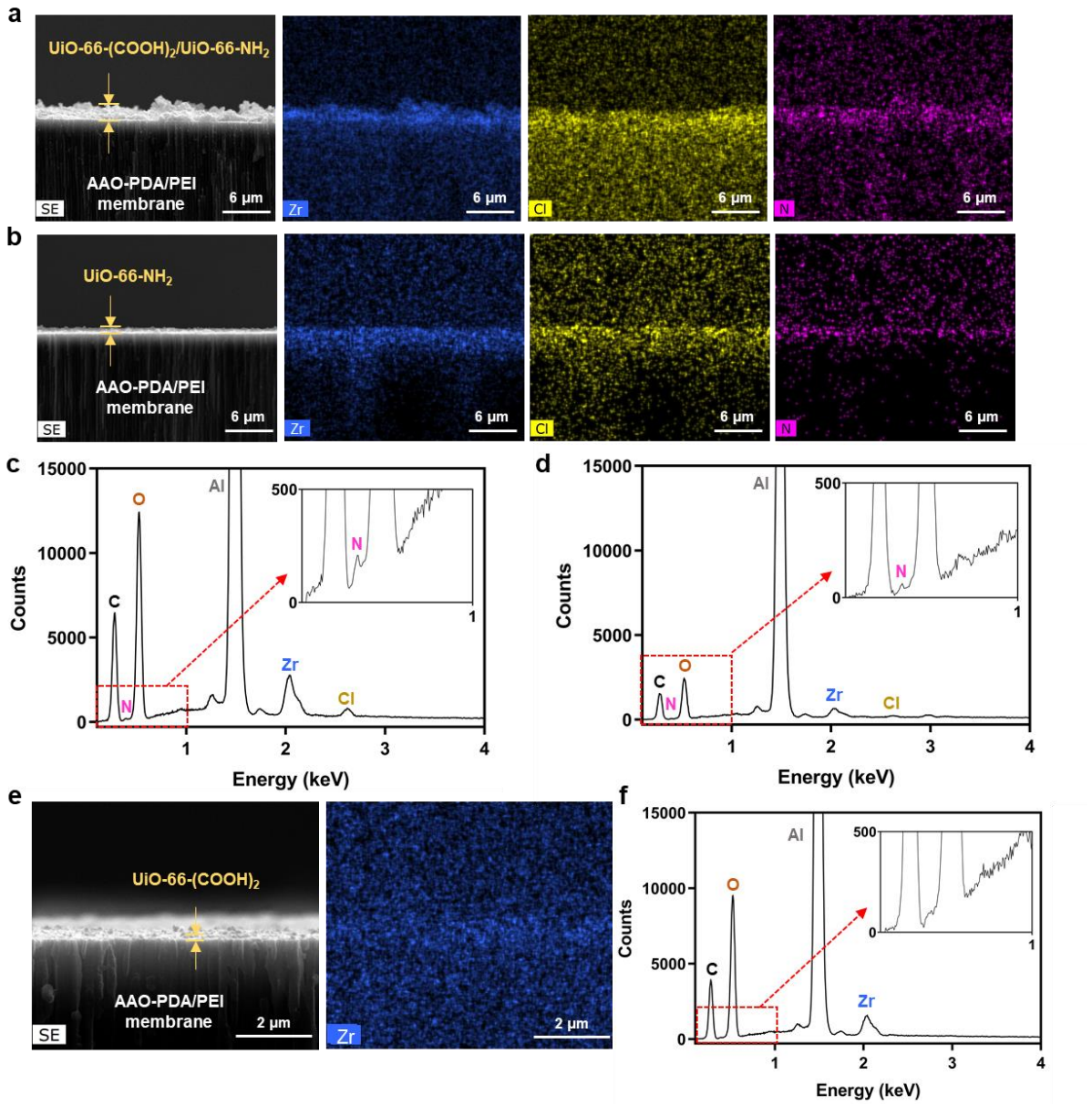

Fig. 3. (a, c) Cross-section image and EDS maps showing Zr, Cl and N elements in the UiO-66-$(COOH)_2$/UiO-66-NH_2 film with corresponding EDS spectrum; (b, d) EDS cross-section image, elemental maps of Zr, Cl and N, and EDS spectrum from a UiO-66-NH_2 membrane; (e, f) EDS cross-section image, elemental map of Zr and EDS spectrum of UiO-66-$(COOH)_2$ seed layer.

EDS mapping of the cross-sections of UiO-66-$(COOH)_2$/UiO-66-NH_2 and UiO-66-NH_2 membranes showed Zr, Cl and N in the UiO-66-$(COOH)_2$/UiO-66-NH_2 and UiO-66-NH_2 films (Fig. 3a and b). All three samples contain Zr, but N and Cl are absent in the UiO-66-$(COOH)_2$ membrane (Fig. 3c, d and f). It indicates that the N and Cl come from the UiO-66-NH_2 layer. Nitrogen can be explained by the presence of -NH_2 in the 2-aminoterephthalate

ligand of UiO-66-NH_2. Nevertheless, the presence of Cl indicates linker deficiencies in UiO-66-NH_2, which may arise due to the replacement of the 2-aminoterephthalate linker by the HCl modulator present in the synthesis solution. This has also been observed in other studies [42-45].

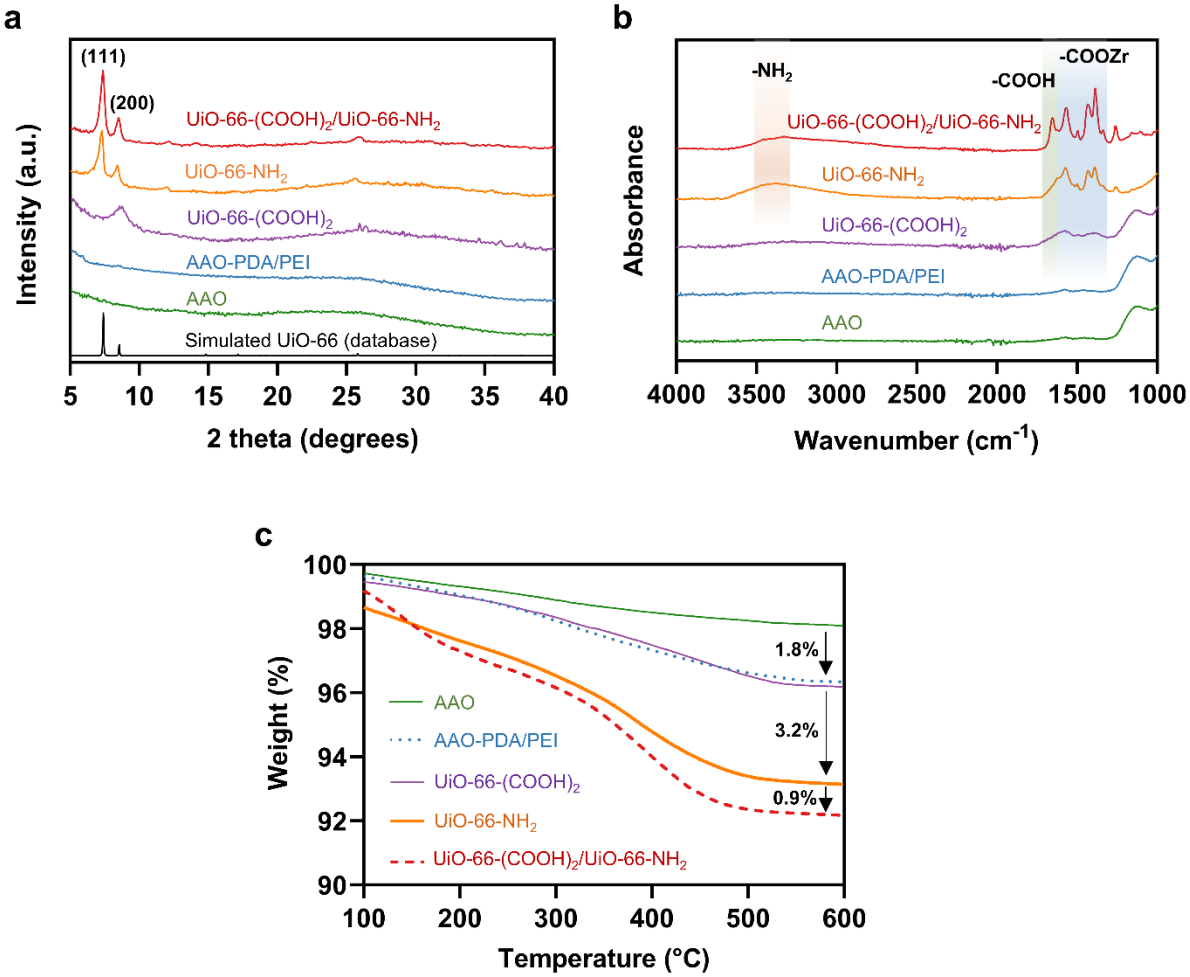

Fig. 4. (a) X-ray diffractograms of AAO, PDA-PEI modified AAO, UiO-66-$(COOH)_2$, UiO-66-NH_2 and UiO-66-$(COOH)_2$/UiO-66-NH_2 membranes, as well as the simulated peaks for UiO-66 (ref ID: 02-002-6797); (b) Surface chemistry analysis via FTIR of AAO, PDA-PEI modified AAO, UiO-66-$(COOH)_2$, UiO-66-NH_2 and UiO-66-$(COOH)_2$/UiO-66-NH_2 membranes; (c) TGA analysis showing degradation and decomposition of AAO, PDA-PEI modified AAO, UiO-66-$(COOH)_2$, UiO-66-NH_2 and UiO-66-$(COOH)_2$/UiO-66-NH_2 membranes.

X-ray diffractometry and FTIR were used to analyze membrane samples further to confirm the underlying synthesis mechanisms of UiO-66-based membranes. X-ray diffractometry showed that the UiO-66-$(COOH)_2$ seed layer has a disordered structure with a

broad peak at 8.6 °2θ (Fig. 4a). The UiO-66-NH_2 membrane showed two distinct peaks at 7.3 °2θ and 8.4 °2θ, which are in accordance with the (111) and (200) planes, respectively. The UiO-66-$(COOH)_2$/UiO-66-NH_2 membrane similarly showed these two distinct peaks corresponding to the simulated UiO-66 pattern from the database. FTIR analysis was carried out to determine the chemical property of the membranes (Fig. 4b). The synthesized UiO-66-$(COOH)_2$ membrane displayed wide absorption bands at 1300-1700 cm^{-1}, corresponding to the carboxylate stretch of the ligand and the free carboxylic acid C=O stretch [46-48]. The weak intensities of these peaks were caused by the preliminary stage of amorphous UiO-66-$(COOH)_2$ growth. At the same time, the UiO-66-NH_2 membrane displayed a broad absorption band at 3300-3500 cm^{-1} attributed to the vibration peaks of an amine functional group in the 2-aminoterephthalate ligand [49]. The peak of the amino-functional group is also presented in the UiO-66-$(COOH)_2$/UiO-66-NH_2 membrane, indicating the successful formation of the UiO-66-NH_2 layer on the UiO-66-$(COOH)_2$ layer. Furthermore, the hybrid membrane revealed a strong absorption peak at 1655 cm^{-1}, corresponding to free carboxylic acid [46]. The absorption peak is attributed to UiO-66-$(COOH)_2$ as a seed layer to promote a continuous and defect-free UiO-66-NH_2 thin film on the membrane and the introduction of UiO-66-NH_2, which promotes UiO-66-$(COOH)_2$ secondary growth.

TGA was also conducted under nitrogen to measure mass loss of the membranes (Fig. 4c). AAO membranes have excellent thermal stability [50], as seen by the relatively minor mass loss of 2% when heated from 100 to 600 °C. A further 1.8% loss of mass for the PDA/PEI modified membrane compared to the pristine AAO membrane when heated to 600 °C, attributed to PDA/PEI decomposition. UiO-66-$(COOH)_2$ formation resulted in a TGA curve comparable to the PDA/PEI membrane, indicating a very thin layer of UiO-66-$(COOH)_2$ on the substrate. However, the synthesis of UiO-66-NH_2 resulted in a 3.2% mass loss compared with the PDA/PEI modified membrane when heated to 600 °C. The rapid loss of mass at ~350 °C reflects the decomposition of organic moieties in UiO-66-NH_2 to form ZrO_2, consistent with earlier studies [49, 51]. The UiO-66-$(COOH)_2$/UiO-66-NH_2 membrane showed a further 0.9% mass loss compared to the UiO-66-NH_2 membrane, indicating a thicker layer of UiO-66-NH_2 with UiO-66-$(COOH)_2$ acting as a seed layer. This is consistent with the observation from cross-sectional SEM images (Fig. 3a, b and e), where the thicknesses of the UiO-66-$(COOH)_2$/UiO-66-NH_2 membrane and UiO-66-NH_2 membrane were estimated to be 1.2±0.2 and 0.5±0.1 μm, respectively.

3.2 Effect of the carboxylic group on Li^+ selectivity under electrical driving force

Current-voltage (*I-V*) measurements were conducted in five electrolyte solutions (LiCl, KCl, NaCl, $MgCl_2$, $CaCl_2$) with 0.01 M ionic strength in the range of -1 to 1 V (Fig. 5) to explore the ion transport behaviors of UiO-66-$(COOH)_2$/UiO-66-NH_2 and UiO-66-NH_2 membranes. *I-V* curves of both membranes in all chloride salt aqueous solutions were symmetric due to the double layered UiO-66s membrane structure symmetry. This indicates these membranes do not have a preferential direction for cations transport. UiO-66 has numerous triangle window apertures (~6 Å), tetrahedral cavities (~8 Å) and octahedral cavities (~11 Å), offering multiple-scale nanochannels accessible to ions [25]. In the case of UiO-66-$(COOH)_2$ and UiO-66-NH_2, the effective pore window and cavity sizes are smaller than the parental UiO-66. Previous studies have determined the pore windows of UiO-66-$(COOH)_2$ and UiO-66-NH_2 to be ~5 Å [52] and ~5.9 Å [53], respectively. The hydrated diameters of the five alkali and alkaline earth metal ions (6.62 Å to 8.56 Å) is bigger than the smallest triangle pore of UiO-66s, so they need to undergo slight changes due to dehydration to pass through these nanochannels [25, 29]. The ionic currents of Li^+ and Mg^{2+} at 1.0 V were 0.0831 mA and 0.001 mA with the UiO-66-$(COOH)_2$/UiO-66-NH_2 membrane (Fig. 5a). On the other hand, the ionic currents of Li^+ and Mg^{2+} at 1 V for the UiO-66-NH_2 membrane were 0.0985 mA and 0.00202 mA, respectively (Fig. 5b). The slopes of Li^+ are higher than the corresponding values for Mg^{2+}, indicating that Li^+ has greater mobility in the nanochannel than Mg^{2+}, which can be attributed to lower hydration energies of Li^+ compared with Mg^{2+} [29]. The slopes of monovalent metal ions are higher than the corresponding values for the divalent ions (Fig. 5c and d). This demonstrates that Li^+, K^+ and Na^+ have higher transmembrane rates than Mg^{2+} and Ca^{2+} due to monovalent ions (6.62 Å to 7.64 Å) having smaller hydrated ionic diameters than divalent metal ions (8.24 Å to 8.56 Å), which enables them to transport faster through the nanochannels of Zr-based membranes.

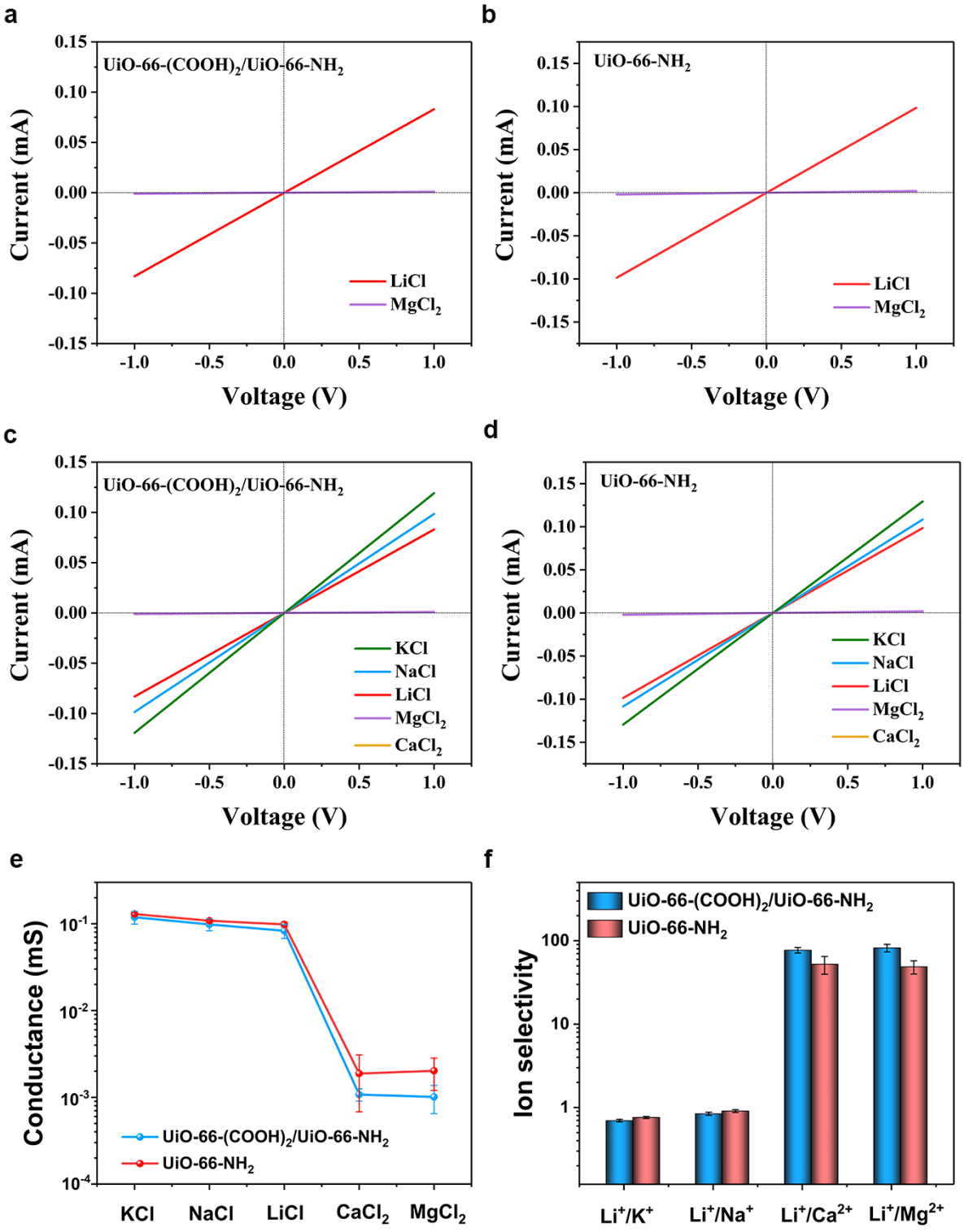

Fig. 5. Metal ion transport behavior in Zr-based membranes via *I-V* measurements. *I-V* curves of (a) UiO-66-$(COOH)_2$/UiO-66-NH_2 membrane and (b) UiO-66-NH_2 membrane were measured in LiCl and $MgCl_2$ aqueous solutions; *I-V* curves of (c) UiO-66-$(COOH)_2$/UiO-66-NH_2 membrane and (d) UiO-66-NH_2 membrane were measured in five electrolyte solutions

(e.g., LiCl, KCl, NaCl, $MgCl_2$, $CaCl_2$); (e) Ionic conductance and (f) metal ion selectivity of two Zr-based membranes measured in five electrolyte solutions with 0.01 M ionic strength.

UiO-66-based membranes with or without carboxylic functional groups have a similar order of ionic conductivity (Fig. 5e). Conductance values of five chloride salts in the UiO-66-NH_2 membrane ranged from 0.0019 to 0.1294 mS which are slightly higher than those of the UiO-66-$(COOH)_2$/UiO-66-NH_2 membrane, which ranged from 0.0010 to 0.1191 mS. The reason could be that these two membranes have similar pore sizes to UiO-66 structure. Conductance values of monovalent chloride salts (K^+, Na^+ and Li^+) in two membranes ranged from 0.08 to 0.13 mS. Conductance values of the divalent alkaline earth ions Ca^{2+} and Mg^{2+}, at 0.00101 to 0.00202 mS, were significantly lower than those of monovalent chloride salts. Differences between the conductivities of monovalent alkali metals and divalent alkali earth metals are related to the higher valence states of Ca^{2+} and Mg^{2+} compared with K^+, Na^+ or Li^+. Both membranes selectively transport alkali metals over alkali earth metals due to the monovalent alkaline ions having a relatively weaker sizing effect with the UiO-66 pore system.

Precisely tuning functional groups in the nanochannels of the membrane is one effective strategy to improve membrane separation performance. A change in the membrane nanochannels for carboxylic groups enhances Li^+ selectivity (Fig. 5f). The separation ratio of Li^+/Mg^{2+} (82.12±8.7) and Li^+/Ca^{2+} (77.13±5.75) in the UiO-66-$(COOH)_2$/UiO-66-NH_2 membrane is significantly higher than those (Li^+/Mg^{2+} (52.34±12.6) and Li^+/Ca^{2+} (48.76±8.9)) of the UiO-66-NH_2 membrane and Li^+/Mg^{2+} (1.37; Fig. S4) of UiO-66-$(COOH)_2$ membrane. Negative surface charges from deprotonation of the carboxylic groups from the media layer (UiO-66-$(COOH)_2$) in the double layered Zr-based membrane offered stronger electrostatic force for divalent metal ions, compared with the positive surface charges from protonation of the amine functional group from the UiO-66-NH_2 membrane [25]. These results indicate carboxylic groups with negative surface charges play an important role in Li^+ selectivity.

3.3 Feed concentration effects on Mg^{2+}/Li^+ selectivity under ion concentration gradients

The dependence of Mg^{2+}/Li^+ selectivity on feed concentrations in aqueous solutions adjacent to nanochannels of the double layered Zr-based membrane with carboxylic groups (UiO-66-$(COOH)_2$/UiO-66-NH_2 membrane) was conducted by varying concentrations of Li^+ and Mg^{2+} ranging from 0.0001 to 0.1 M (Fig. 6). Ionic permeation rates are proportional to the feed concentrations of ions at higher concentrations, but ion transport behaviors are different

at lower concentrations. At the low cation feed concentration of 0.0001 M, the membrane exhibited a stronger electrostatic force repulsion for Mg^{2+} than Li^{+}. Li^{+} could transport through the membrane more easily than Mg^{2+} at 0.0001 M, and the Mg^{2+}/Li^{+} molar ratio in the permeate was 0.873. This ratio is attributed to the surface-charge-governed transport behavior in nanochannels and electric double layer (EDL) overlaps at lower concentrations [12, 54].

With the increasing molar ratio of Mg^{2+}/Li^{+} in the feed side, the increase in solution molar concentration leads to an increase in ionic strength (I) and a decrease in the thickness of EDL ($\lambda_D = \frac{0.304}{\sqrt{I}}$ At 25 ºC) [17, 55]. EDL on the nanochannels of UiO-66-$(COOH)_2$/UiO-66-NH_2 membrane becomes more compressed and offers wider channels for Mg and Li transport. Under concentration gradient driving force, Mg^{2+}/Li^{+} selectivity of the UiO-66-$(COOH)_2$/UiO-66-NH_2 membrane dramatically increases with an increasing Mg^{2+}/Li^{+} molar ratio in the feed side. The Mg^{2+}/Li^{+} selectivity was up to 11.89 with a feed Mg^{2+}/Li^{+} molar ratio of 10 at 5 h (C_{Mg2+} = 0.1 M and C_{Li+} = 0.01 M) and reached up to 15.2 with a feed Mg^{2+}/Li^{+} molar ratio of 100 at 5 h (initial C_{Mg2+} = 0.1 M and C_{Li+} = 0.0001 M). The reason could be that Mg can present into two states, including Mg^{2+} and $MgCl^{+}$, and the fraction of the $MgCl^{+}$ ion pair in aqueous solution increases with a rising Mg^{2+}/Li^{+} molar ratio in the feed side [4]. $MgCl^{+}$ ion pairs owing to their lower positive charge density and larger sizes than Mg^{2+} ions, are easier to transport through the positively charged UiO-66-NH_2 layer on the membrane surface and then stronger electro-migration in the UiO-66-$(COOH)_2$ media layer of the membrane with fixed carboxylic groups.

The UiO-66-$(COOH)_2$/UiO-66-NH_2 membrane exhibited a higher selectivity for high concentrations of Mg^{2+} with a low concentration of Li^{+} as feed solution. Its Mg^{2+}/Li^{+} selectivity was 2.93 times that of UiO-66-NH_2 membrane (5.18 at 5 h; Fig. S4) for an initial Mg^{2+}/Li^{+} molar ratio of 100 (initial C_{Mg2+} = 0.1 M and C_{Li+} = 0.0001 M). Based on these above results, the double layered Zr-based membranes with carboxylic functional groups hold promise for lithium recovery from brines containing a high Mg^{2+}/Li^{+} ratio under a concentration gradient.

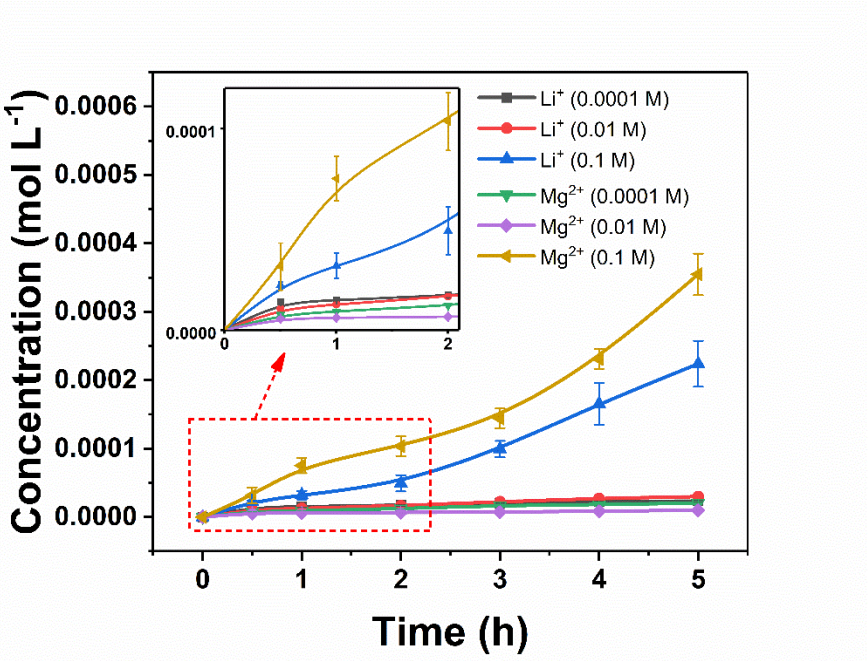

Fig. 6. Concentrations of Li^+ and Mg^{2+} in permeation solutions at the interval with varying feed concentrations of LiCl and $MgCl_2$ aqueous solutions in a range of 0.0001 to 0.1 M with the double layered Zr-based membrane.

3.4 Effect of driving force for lithium recovery from brine

Comparison of different brines (Table 1) shows that Li^+ concentrations vary from 0.0008213 to 0.121 mol L^{-1} and Mg^{2+}/Li^+ molar ratios vary from 1.76 to 200.38. We selected a typical Taijiner brine containing Li^+, Na^+, K^+, Ca^{2+}, Mg^{2+} and with a Mg^{2+}/Li^+ molar ratio of 20.75 to further evaluate the operating performance of the double layered Zr-based membrane. Mg^{2+}/Li^+ separation performance of the UiO-66-$(COOH)_2$/UiO-66-NH_2 membrane in synthetic Taijiner brine was evaluated under two different driving forces, including electrical potential difference (ΔE) and concentration difference (ΔC).

Fig. 7a shows metal ion transport behavior across the Zr-based membrane with carboxylic groups in the synthetic Taijiner brine under these two driving forces. Li^+ and Mg^{2+} in aqueous solutions present as hydrated ions with diameters of 7.64 Å and 8.56 Å for Li^+ and Mg^{2+} respectively [29]. The UiO-66-$(COOH)_2$/UiO-66-NH_2-AAO membrane has triangular-shaped windows less than 6 Å diameter, which is relatively smaller than the hydrated ionic sizes of Li^+ and Mg^{2+} ions but bigger than their ionic diameters (Fig. 7b). So, for Li^+ and Mg^{2+} ions to enter the pore structure of the Zr-based membrane, they must be in a dehydrated state

and then rehydrate to exit the pore into the aqueous solution. Driven by the applied voltage, the ion mobility of Li^+ inside nanochannels could be larger than Mg^{2+} due to a more compact shell of partially dehydrated Li^+ with a smaller size than Mg^{2+} [12, 56]. In contrast, the mobility of Li^+ under concentration gradient-driven force is lower than its mobility under electrical-driven force. Infiltration of Li^+ could be easily captured or attracted by negatively charged -$(COOH)_2$ and less repelled by Zr^{4+} repulsive force relative to Mg^{2+} [57, 58].

Fig. 7c and d show the permeation behavior of metal ions and ion selectivity in synthetic Taijiner brine. The selectivity order of metal ions is $K^+>Na^+>Li^+>Mg^{2+}>Ca^{2+}$ under the electrical-driven force and $K^+>Na^+>Mg^{2+}>Ca^{2+}>Li^+$ under the concentration gradient, respectively. According to the Eisenman sequence (Sequence I) at low anionic field strength, the ion selectivity order is $K^+>Na^+>Li^+$ as Li^+ has relatively greater hydration energy [12]. Interestingly, a low concentration of Li^+ ions in brine exhibited a lower transport speed than that of Mg^{2+} moving through nanochannels of the UiO-66-$(COOH)_2$/UiO-66-NH_2 membrane under concentration gradients. Compared with Mg ions, Li ions can more easily enter the nanochannel openings of the double layered Zr-based membrane. However, Li^+ needs to overcome many energy barriers and binding sites from carboxylic groups of UiO-66-$(COOH)_2$, slowing its transport rate in the nanochannels. The normalized selectivity ratio of Mg^{2+}/Li^+ is 0.5 (Fig. 7c) under electric potential gradient driving force and the ratio increases to 10 (Fig. 7d) under concentration gradient driving force. This indicates that double layered Zr-based membrane with carboxylic groups displayed greater selectivity for Mg^{2+}/Li^+ and lower energy consumption under concentration gradient driving force.

Stability and recycling ability are essential characteristics to evaluate membrane working performance for industrial applications. Long-term filtration tests driven by concentration gradients were conducted to study the stability of the UiO-66-$(COOH)_2$/UiO-66-NH_2 membrane. This membrane exhibited an excellent recycling ability and stability within 72 hours and a slight decrease in the normalized selectivity ratio of Mg^{2+} and Li^+ to 6.7 (Fig. S5) with 7-day continuous filtration driven by a concentration gradient. These membrane samples were characterized by SEM and XRD to further demonstrate the structural stability of the UiO-66-$(COOH)_2$/UiO-66-NH_2 membrane. However, SEM images comparing Fig. 2 with Fig. S6a, b reveal minor morphological variation and voids on the membrane surface. The XRD patterns of membranes remain the characteristic peaks after the long-term operation (Fig. S6c). Thus, the UiO-66-$(COOH)_2$/UiO-66-NH_2 AAO membrane exhibited excellent separation

performance for Mg^{2+}/Li^{+} from natural brine containing a high Mg^{2+}/Li^{+} ratio under a concentration gradient.

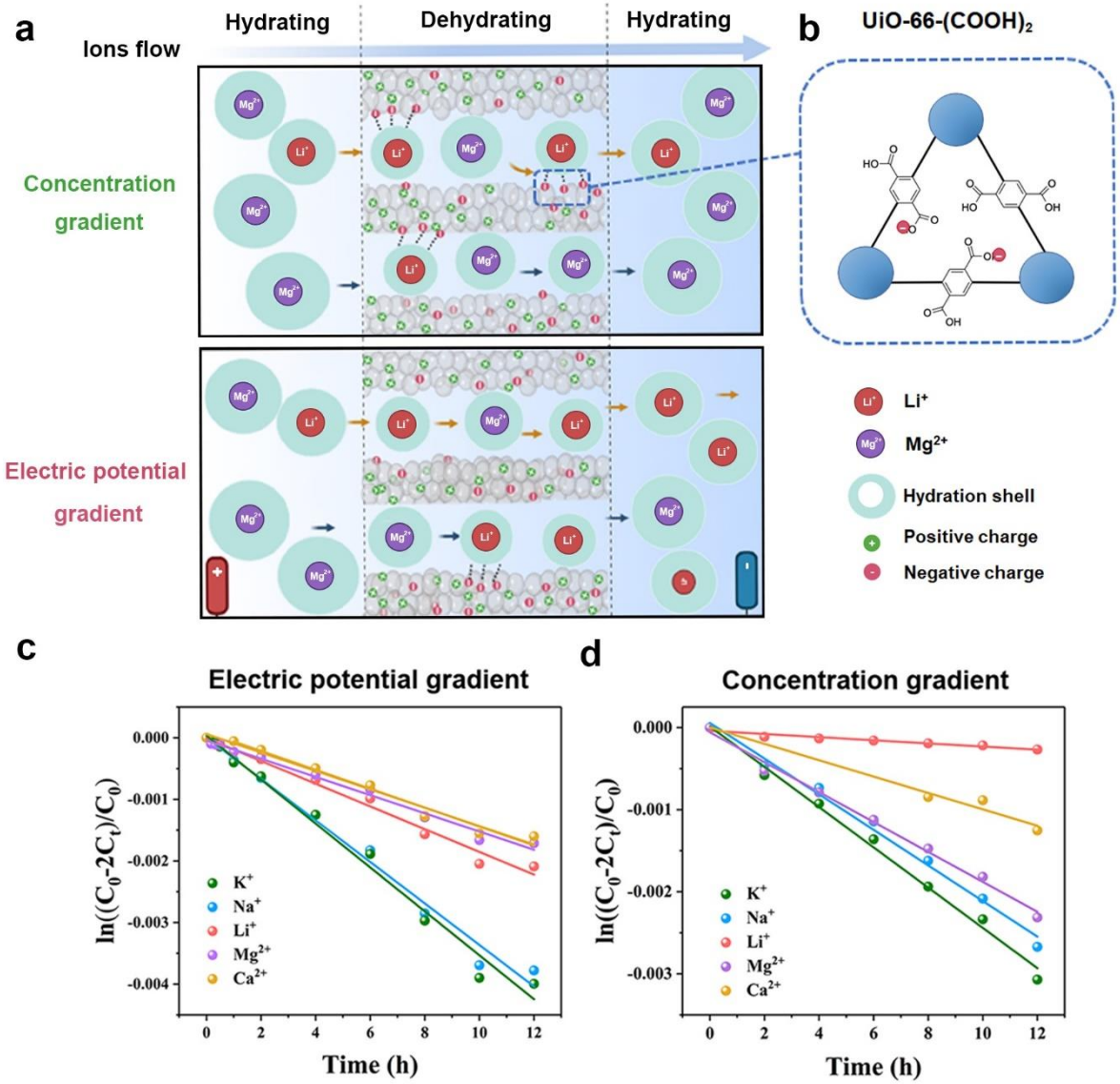

Fig. 7. Schematic of a double layered Zr-based membrane (UiO-66-$(COOH)_2$/UiO-66-NH_2 AAO membrane) for Li^{+} extraction from brine (a) under different driving forces and (b) chemical structure of the UiO-66-$(COOH)_2$ triangular-shaped pore. Plots of $\ln((C_0-2C_t)/C_0)$ vs. time (feed solution is synthetic Taijiner brine) under (c) voltage and (d) concentration gradients over 12 h.

4. Conclusions

This study proposed a facile method of UiO-66-$(COOH)_2$/UiO-66-NH_2 AAO membrane via seed-assisted in situ growth for lithium recovery from synthetic Taijiner brine containing a high Mg^{2+}/Li^+ ratio. Compared with the UiO-66-NH_2 membrane, the double layered UiO-66-based membrane with carboxylic groups exhibited relatively higher selectivity for monovalent ions than divalent metal ions under an electrically-driven process. After investigation of feed concentration effects, this double layered membrane with carboxylic groups displayed a much better selectivity at a relatively higher Mg^{2+}/Li^+ molar ratio of feed. Under a concentration gradient, this membrane exhibited better performance for Mg^{2+}/Li^+ separation in synthetic Taijiner brine due to the need for partially dehydrated Li^+ to overcome more energy barriers and binding sites from carboxylic groups. This research will inspire future work for MOF-on-MOF membrane preparation and offer a guideline for enhanced lithium enrichment from commercial or natural brine resources with artificial nanostructured membranes using an energy-efficient process.

Declaration of competing interest

The authors declare no conflict of interest.

Acknowledgments

Authors acknowledge financial support provide by the UTS CPRDF award (PRO20-11072), the Australian Research Council-Discovery Early Career Researcher Award (DECRA) DE180100688 and the ARC Discovery project 180103874.

References

[1] X. Li, Y. Mo, W. Qing, S. Shao, C.Y. Tang, J. Li, Membrane-based technologies for lithium recovery from water lithium resources: A review, J. Membr. Sci. 591 (2019) 117317.
[2] B. Swain, Separation and purification of lithium by solvent extraction and supported liquid membrane, analysis of their mechanism: a review, J. Chem. Technol. Biotechnol. 91 (2016) 2549-2562.
[3] B. Swain, Recovery and recycling of lithium: A review, Sep. Purif. Technol. 172 (2017) 388-403.
[4] Y. Zhang, L. Wang, W. Sun, Y. Hu, H. Tang, Membrane technologies for Li+/Mg2+ separation from salt-lake brines and seawater: A comprehensive review, J. Ind. Eng. Chem. 81 (2020) 7-23.

[5] X. Zhu, H. Yue, W. Sun, L. Zhang, Q. Cui, H. Wang, Study on adsorption extraction process of lithium ion from West Taijinar brine by shaped titanium-based lithium ion sieves, Sep. Purif. Technol. 274 (2021) 119099.
[6] T. Hoshino, Preliminary studies of lithium recovery technology from seawater by electrodialysis using ionic liquid membrane, Desalination 317 (2013) 11-16.
[7] T. Hoshino, T. Terai, Basic technology for 6Li enrichment using an ionic-liquid impregnated organic membrane, J. Nucl. Mater. 417 (2011) 696-699.
[8] P.K. Choubey, K.S. Chung, M.S. Kim, J.C. Lee, R.R. Srivastava, Advance review on the exploitation of the prominent energy-storage element Lithium. Part II: From sea water and spent lithium ion batteries (LIBs), Miner. Eng. 110 (2017) 104-121.
[9] P.K. Choubey, M.S. Kim, R.R. Srivastava, J.C. Lee, J.Y. Lee, Advance review on the exploitation of the prominent energy-storage element: Lithium. Part I: From mineral and brine resources, Miner. Eng. 89 (2016) 119-137.
[10] P. Meshram, B.D. Pandey, T.R. Mankhand, Extraction of lithium from primary and secondary sources by pre-treatment, leaching and separation: A comprehensive review, Hydrometallurgy 150 (2014) 192-208.
[11] X. Y. Nie, S. Y. Sun, Z. Sun, X. Song, J. G. Yu, Ion-fractionation of lithium ions from magnesium ions by electrodialysis using monovalent selective ion-exchange membranes, Desalination 403 (2017) 128-135.
[12] A. Razmjou, M. Asadnia, E. Hosseini, A. Habibnejad Korayem, V. Chen, Design principles of ion selective nanostructured membranes for the extraction of lithium ions, Nat. Commun. 10 (2019) 5793.
[13] A. Razmjou, G. Eshaghi, Y. Orooji, E. Hosseini, A.H. Korayem, F. Mohagheghian, Y. Boroumand, A. Noorbakhsh, M. Asadnia, V. Chen, Lithium ion-selective membrane with 2D subnanometer channels, Water Res. 159 (2019) 313-323.
[14] R. Taheri, A. Razmjou, G. Szekely, J. Hou, G.R. Ghezelbash, Biodesalination-on harnessing the potential of nature's desalination processes, Bioinspir. Biomim. 11 (2016) 041001.
[15] T. Hoshino, Innovative lithium recovery technique from seawater by using world-first dialysis with a lithium ionic superconductor, Desalination 359 (2015) 59-63.
[16] H. Xiao, H. Zhou, S. Feng, D.B. Gore, Z. Zhong, W. Xing, In situ growth of two-dimensional ZIF-L nanoflakes on ceramic membrane for efficient removal of iodine, J. Membr. Sci. 619 (2021) 118782.
[17] H. Ahmadi, E. Hosseini, W. Cha-Umpong, M. Abdollahzadeh, A.H. Korayem, A. Razmjou, V. Chen, M. Asadnia, Incorporation of natural lithium-ion trappers into graphene oxide nanosheets, Adv. Mater. Technol. 6 (2021) 2000665.
[18] A. Razmjou, E. Hosseini, W. Cha-Umpong, A.H. Korayem, M. Asadnia, P. Moazzam, Y. Orooji, H. Karimi-Maleh, V. Chen, Effect of chemistry and geometry of GO nanochannels on the Li ion selectivity and recovery, Desalination 496 (2020) 114729.

[19] Y. Sun, Q. Wang, Y. Wang, R. Yun, X. Xiang, Recent advances in magnesium/lithium separation and lithium extraction technologies from salt lake brine, Sep. Purif. Technol. 256 (2021) 117807.
[20] N. Stock, S. Biswas, Synthesis of Metal-Organic Frameworks (MOFs): Routes to various MOF topologies, morphologies, and composites, Chem. Rev. 112 (2012) 933-969.
[21] J. Yao, H. Wang, Zeolitic imidazolate framework composite membranes and thin films: synthesis and applications, Chem. Soc. Rev. 43 (2014) 4470-4493.
[22] B. Seoane, J. Coronas, I. Gascon, M.E. Benavides, O. Karvan, J. Caro, F. Kapteijn, J. Gascon, Metal-organic framework based mixed matrix membranes: a solution for highly efficient CO2 capture?, Chem. Soc. Rev. 44 (2015) 2421-2454.
[23] Y. S. Li, H. Bux, A. Feldhoff, G. L. Li, W. S. Yang, J. Caro, Controllable synthesis of metal-organic frameworks: From MOF nanorods to oriented MOF membranes, Adv. Mater. 22 (2010) 3322-3326.
[24] H. Xiao, Z.X. Low, D.B. Gore, R. Kumar, M. Asadnia, Z. Zhong, Porous metal-organic framework-based filters: Synthesis methods and applications for environmental remediation, Chem. Eng. Sci. (2021) 133160.
[25] H. Zhang, J. Hou, Y. Hu, P. Wang, R. Ou, L. Jiang, J.Z. Liu, B.D. Freeman, A.J. Hill, H. Wang, Ultrafast selective transport of alkali metal ions in metal organic frameworks with subnanometer pores, Sci. Adv. 4 (2018) eaaq0066.
[26] Z. Zhang, P. Zhang, S. Yang, T. Zhang, M. Löffler, H. Shi, M.R. Lohe, X. Feng, Oxidation promoted osmotic energy conversion in black phosphorus membranes, Proc. Natl. Acad. Sci. 117 (2020) 13959.
[27] J. Lu, H. Zhang, J. Hou, X. Li, X. Hu, Y. Hu, C.D. Easton, Q. Li, C. Sun, A.W. Thornton, M.R. Hill, X. Zhang, G. Jiang, J.Z. Liu, A.J. Hill, B.D. Freeman, L. Jiang, H. Wang, Efficient metal ion sieving in rectifying subnanochannels enabled by metal-organic frameworks, Nat. Mater. 19 (2020) 767-774.
[28] J. Lu, H. Zhang, X. Hu, B. Qian, J. Hou, L. Han, Y. Zhu, C. Sun, L. Jiang, H. Wang, Ultraselective monovalent metal ion conduction in a three-dimensional sub-1 nm nanofluidic device constructed by metal-organic frameworks, ACS Nano, 15 (2021) 1240-1249.
[29] C. Zhang, Y. Mu, W. Zhang, S. Zhao, Y. Wang, PVC-based hybrid membranes containing metal-organic frameworks for Li+/Mg2+ separation, J. Membr. Sci. 596 (2020) 117724.
[30] T. Xu, M.A. Shehzad, X. Wang, B. Wu, L. Ge, T. Xu, Engineering Leaf-Like UiO-66-SO3H Membranes for Selective Transport of Cations, Nanomicro Lett. 12 (2020) 51.
[31] T. Xu, M.A. Shehzad, D. Yu, Q. Li, B. Wu, X. Ren, L. Ge, T. Xu, Highly Cation Permselective Metal-Organic Framework Membranes with Leaf-Like Morphology, ChemSusChem. 12 (2019) 2593-2597.

[32] T. Xu, F. Sheng, B. Wu, M.A. Shehzad, A. Yasmin, X. Wang, Y. He, L. Ge, X. Zheng, T. Xu, Ti-exchanged UiO-66-NH2–containing polyamide membranes with remarkable cation permselectivity, J. Membr. Sci. 615 (2020) 118608.
[33] Y. Guo, Y. Ying, Y. Mao, X. Peng, B. Chen, Polystyrene sulfonate threaded through a metal-organic framework membrane for fast and selective lithium-ion separation, Angew. Chem. Int. Ed. 55 (2016) 15120-15124.
[34] M. Abdollahzadeh, M. Chai, E. Hosseini, M. Zakertabrizi, M. Mohammad, H. Ahmadi, J. Hou, S. Lim, A. Habibnejad Korayem, V. Chen, M. Asadnia, A. Razmjou, Designing angstrom-scale asymmetric MOF-on-MOF cavities for high monovalent ion selectivity, Adv. Mater. (2021) 2107878.
[35] H. Dou, M. Xu, B. Wang, Z. Zhang, G. Wen, Y. Zheng, D. Luo, L. Zhao, A. Yu, L. Zhang, Z. Jiang, Z. Chen, Microporous framework membranes for precise molecule/ion separations, Chem. Soc. Rev. 50 (2021) 986-1029.
[36] S. Y. Sun, L. J. Cai, X. Y. Nie, X. Song, J. G. Yu, Separation of magnesium and lithium from brine using a Desal nanofiltration membrane, J. Water Process. Eng. 7 (2015) 210-217.
[37] J.W. An, D.J. Kang, K.T. Tran, M.J. Kim, T. Lim, T. Tran, Recovery of lithium from Uyuni salar brine, Hydrometallurgy 117-118 (2012) 64-70.
[38] W. Cha-umpong, Q. Li, A. Razmjou, V. Chen, Concentrating brine for lithium recovery using GO composite pervaporation membranes, Desalination 500 (2021) 114894.
[39] M. Mohammad, A. Razmjou, K. Liang, M. Asadnia, V. Chen, Metal-organic-framework-based enzymatic microfluidic biosensor via surface patterning and biomineralization, ACS Appl. Mater. Interfaces 11 (2018) 1807-1820.
[40] M. Chai, A. Razmjou, V. Chen, Metal-organic-framework protected multi-enzyme thin-film for the cascade reduction of CO2 in a gas-liquid membrane contactor, J. Membr. Sci. (2021) 118986.
[41] X.P. Wang, J. Hou, F.S. Chen, X.M. Meng, In-situ growth of metal-organic framework film on a polydopamine-modified flexible substrate for antibacterial and forward osmosis membranes, Sep. Purif. Technol. 236 (2020) 116239.
[42] F. Vermoortele, B. Bueken, G.l. Le Bars, B. Van de Voorde, M. Vandichel, K. Houthoofd, A. Vimont, M. Daturi, M. Waroquier, V. Van Speybroeck, Synthesis modulation as a tool to increase the catalytic activity of metal-organic frameworks: the unique case of UiO-66 (Zr), J. Am. Chem. Soc. 135 (2013) 11465-11468.
[43] G.C. Shearer, S. Chavan, S. Bordiga, S. Svelle, U. Olsbye, K.P. Lillerud, Defect engineering: tuning the porosity and composition of the metal-organic framework UiO-66 via modulated synthesis, Chem. Mater. 28 (2016) 3749-3761.
[44] M. Vandichel, J. Hajek, F. Vermoortele, M. Waroquier, D.E. De Vos, V. Van Speybroeck, Active site engineering in UiO-66 type metal-organic frameworks by intentional creation of defects: a theoretical rationalization, CrystEngComm, 17 (2015) 395-406.

[45] G.C. Shearer, S. Chavan, J. Ethiraj, J.G. Vitillo, S. Svelle, U. Olsbye, C. Lamberti, S. Bordiga, K.P. Lillerud, Tuned to perfection: ironing out the defects in metal-organic framework UiO-66, Chem. Mater. 26 (2014) 4068-4071.
[46] Y. Luan, Y. Qi, Z. Jin, X. Peng, H. Gao, G. Wang, Synthesis of a flower-like Zr-based metal-organic framework and study of its catalytic performance in the Mannich reaction, RSC Adv. 5 (2015) 19273-19278.
[47] G. Yalcin, A. Kayan, Synthesis and characterization of Zr, Ti, Al-phthalate and pyridine-2-carboxylate compounds and their use in ring opening polymerization, Appl. Catal. A Gen. 433 (2012) 223-228.
[48] E. Binaeian, Y. Li, H.-A. Tayebi, D. Yuan, Enhancing toxic gas uptake performance of Zr-based MOF through uncoordinated carboxylate and copper insertion; ammonia adsorption, J. Hazard. Mater. 416 (2021) 125933.
[49] Y. Cao, H. Zhang, F. Song, T. Huang, J. Ji, Q. Zhong, W. Chu, Q. Xu, UiO-66-NH2/GO composite: synthesis, characterization and CO2 adsorption performance, Materials 11 (2018) 589.
[50] X. Huang, H. Mutlu, P. Théato, The toolbox of porous anodic aluminum oxide-based nanocomposites: from preparation to application, Colloid Polym. Sci. 299 (2021) 325-341.
[51] M. K. Kim, S.H. Kim, M. Park, S.G. Ryu, H. Jung, Degradation of chemical warfare agents over cotton fabric functionalized with UiO-66-NH2, RSC adv. 8 (2018) 41633-41638.
[52] Z. Hu, Y. Peng, Z. Kang, Y. Qian, D. Zhao, A modulated hydrothermal (MHT) approach for the facile synthesis of UiO-66-type MOFs, Inorg. Chem. 54 (2015) 4862-4868.
[53] X. Li, H. Zhang, P. Wang, J. Hou, J. Lu, C.D. Easton, X. Zhang, M.R. Hill, A.W. Thornton, J.Z. Liu, Fast and selective fluoride ion conduction in sub-1-nanometer metal-organic framework channels, Nat. Comm. 10 (2019) 1-12.
[54] C. Wang, F. F. Liu, Z. Tan, Y. M. Chen, W. C. Hu, X. H. Xia, Fabrication of bio-inspired 2D MOFs/PAA hybrid membrane for asymmetric ion transport, Adv. Func. Mater. 30 (2020) 1908804.
[55] F. Arshadi, M. Mohammad, E. Hosseini, H. Ahmadi, M. Asadnia, Y. Orooji, A.H. Korayem, A. Noorbakhsh, A. Razmjou, The effect of D-spacing on the ion selectivity performance of MXene membrane, J. Membr. Sci. 639 (2021) 119752.
[56] Q. Wen, D. Yan, F. Liu, M. Wang, Y. Ling, P. Wang, P. Kluth, D. Schauries, C. Trautmann, P. Apel, W. Guo, G. Xiao, J. Liu, J. Xue, Y. Wang, Highly selective ionic transport through subnanometer pores in polymer films, Adv. Funct. Mater. 26 (2016) 5796-5803.
[57] G.M. Geise, D.R. Paul, B.D. Freeman, Fundamental water and salt transport properties of polymeric materials, Prog. Polym. Sci. 39 (2014) 1-42.
[58] S.H. Park, K. Kim, J.H. Lim, S.J. Lee, Selective lithium and magnesium adsorption by phosphonate metal-organic framework-incorporated alginate hydrogel inspired from lithium adsorption characteristics of brown algae, Sep. Purif. Technol. 212 (2019) 611-618.